PVP-Assisted Hydrothermal Synthesis of Bi_2O_2Se Nanosheets for Self-Powered Photodetector

Xiang Yu Zhang, Dongbo Wang[*], Zhi Zeng, Chenchen Zhao, Yaxin Liu, Bingke Zhang, Jingwen Pan, Donghao Liu and Jinzhong Wang[*]

Department of Optoelectronic Information Science, School of Materials Science and Engineering, Harbin Institute of Technology, Harbin 150001, China

Abstract: Bi_2O_2Se nanosheets were successfully synthesized via a facile one-step PVP-assisted hydrothermal process for the first time. Corresponding characterizations, such as XRD, XPS, SEM and TEM, were carried out to investigate the formation of the products on the amount of PVP in the reaction system. Results revealed that the single-crystalline Bi_2O_2Se nanosheets with small mean lateral size of 176.3 nm were obtained when the amount of PVP is 0.75 g. Single-crystalline Bi_2O_2Se nanosheets self-powered photodetector exhibited excellent photodetection performance, superior to that of self-powered photodetectors based on the products synthesized without PVP and other nanomaterials. Under the illumination of 365 nm ultraviolet light, the rise time, responsivity and detectivity could approach up to 9 ms, 14.24 mA/W and 3.16×10^8 Jones, respectively. Bi_2O_2Se devices have high photoresponse even in the visible and near infrared bands due to its suitable band gap. The present work provides a novel preparation route of Bi_2O_2Se via hydrothermal method and PVP assisted synthesis of Bi_2O_2Se nanosheets is reported for the first time. Bi_2O_2Se nanosheets self-powered photodetector exhibited excellent photodetection performance and points out a direction for the evolution of self-powered photodetectors in the in the future.

Keywords: Bi_2O_2Se, Nanosheets, PVP, Hydrothermal, Self-powered.

1. INTRODUCTION

In recent years, self-powered photodetectors have attracted great interest among researchers due to environmental friendliness and simple fabrication, which play a vital role in the aspects of military, communication, gas sensor and biomedical imaging [1-4]. In comparison with conventional photodetectors, self-powered photodetectors not only exhibit the excellent photodetection performance with high photoresponsivity and fast photoresponse rate, but also can work without external power, which meets the need of photodetection in a variety of complex environments [5-6].

However, the inherent characteristics of traditional semiconductor nanomaterials, such as graphene's relatively low absorbance, MoS_2's slow response speed and BP' environmental instability, limited their further application in the field of self-powered photodetectors [7-9]. Bi_2O_2Se has emerged as a promising new semiconductor material with excellent optoelectronic properties. It was reported that photodetectors based on Bi_2O_2Se demonstrate a perfectly comprehensive performance consisting of the high electron mobility, ultrasensitive photoresponse and outstanding environmental stability [10].

Furthermore, Bi_2O_2Se possesses a moderate band gap (≈0.8 eV), which realizes photodetection over a wide spectral range from ultraviolet light to near-infrared light. Based on these reasons, Bi_2O_2Se is considered as an ideal candidate of next generation optoelectronic devices [11-12].

Normally, Bi_2O_2Se nanosheets were synthesized by a facile hydrothermal method using $Bi(NO_3)_3 \cdot 5 H_2O$ as Bi source and Se power as Se source. However, Bi_2O_2Se nanosheets reported to date maintain a relatively large size with the lateral dimension of several micron, to some extent leading to a poor photoelectric performance and limiting the development of the self-powered photodetectors based on Bi_2O_2Se nanosheets. In order to enhance the material's performance, considerable efforts have been devoted to the fabrication of nanomaterials with different morphologies as a reference of the grown of Bi_2O_2Se nanosheets. For instance, Liang *et al*. have obtained MoS_2 nanosheets by PVP-assisted hydrothermal reaction with improved lithium storage properties [13]. Ding *et al*. have synthesized single-crystalline $Bi_2O_2SiO_3$ nanosheets via a facile one-step CTAB-assisted hydrothermal method with superior photocatalytic performances [14]. Wang *et al*. have demonstrated PVP-assisted synthesized Sb_2S_3 nanowire with good photoresponse properties [15].

In this work, an efficient and scalable strategy has been developed for the PVP-assisted synthesis of Bi_2O_2Se nanosheets via a hydrothermal reaction. The

*Address correspondence to this author at the Department of Optoelectronic Information Science, School of Materials Science and Engineering, Romania; Tel: +86-0451-86418329; E-mail: wangdongbo@hit.edu.cn, jinzhong_wang@hit.edu.cn

obtained Bi_2O_2Se nanosheets were characterized by XRD, XPS, SEM and TEM, to explain the effects of PVP content on the formation and morphology. The performance of self-power photodetector based on Bi_2O_2Se products was discussed in detail. It is hoped that this study would provide a new preparation route of Bi_2O_2Se nanosheets via hydrothermal method and facilitate the development of novel type self-power photodetector in the future.

2. EXPERIMENTAL SECTION

2.1. Materials

Bismuth nitrate pentahydrate ($Bi(NO_3)_3 \cdot 5H_2O$ 99.99%), Se power (Se, 99.99%), Lithium nitrate ($LiNO_3$, 99%), Sodium hydroxide (NaOH, 96%), Sodium sulfite (Na_2SO_3, 98%) were purchased from Aladdin. PVP (K30, $M_w \approx 40,000$) was purchased from Sigma-Aldrich. Potassium nitrate (KNO_3, 99%) was purchased from Tianjin Fengchuan Chemical Reagent Co., Ltd. All the reagents were of analytical grade and used as received without further purification.

In this study, Bi_2O_2Se nanosheets were synthesized by one-step hydrothermal method. Briefly, 1 mmol Bi $(NO_3)_3 \cdot 5H_2O$ and 0.25 g PVP were dissolved in 20 mL deionized water denoted as solution A. 3.0 g $LiNO_3$ and 6.0 g KNO_3 were then added to solution A to stir at constant temperature until being completely dissolved. Meanwhile, 0.5 mmol Se power and 0.15 g Na_2SO_3 were dissolved in 20 mL deionized water and were heated for 0.5 h denoted as solution B. The PH value of solution B was adjusted by the addition of 1.0 g NaOH. Subsequently, solution B was slowly added to solution A with constant stirring for 0.5 h and a brown suspension was obtained. The suspension was transferred to a 100 mL Teflon-lined stainless-steel vessel, which was heated at 200 °C for 24 h under autogenous pressure in an oven. when cooling down to room temperature, the product was collected and washed with deionized water and ethanol for several times, then dried under vacuum at 60 °C for 6 h. Products adding different amounts of PVP (x = 0.0, 0.25, 0.50, 0.75 mmol) were prepared according to this method (similar procedure) and were marked as BP-0, BP-1, BP-2, and BP-3, respectively.

2.2. Device Fabrication

The ITO substrate was ultrasonically cleaned in acetone, anhydrous ethanol and deionized water for 30 min, respectively. The as-produced Bi_2O_2Se nanosheets were uniformly coated in the conductive layer surface of the cleaned ITO substrate as a working electrode. Subsequently, the working electrode, polysulfide electrolyte (0.5 M Na_2S, 2 M S, and 0.2 M KCl were dissolved in a methanol/water (7:3 by volume) solution) and the platinum electrode was sealed at 150 ℃ as a Bi_2O_2Se nanosheets self-powered photodetector to use.
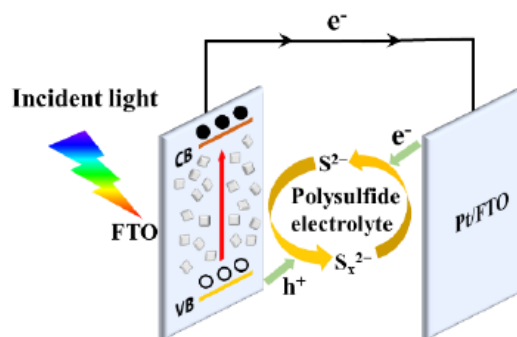
Scheme 1: Illustration of as-fabricated PEC-type self-powered photodetector.

2.3. Characterization

The crystal structure and phase composition of the samples were demonstrated by X-ray diffraction (XRD, Panalytical Empyrean) with Cu-Kα radiation over the 2θ range from 20° to 70°. The surface morphology of Bi_2O_2Se nanosheets was characterized using a field emission scanning electron microscope (FESEM, Zeiss) at a 20 kV accelerating voltage. Transmission electron microscopy (TEM, JEM-F200) and high-resolution transmission electron microscope (HRTEM) were adopted to characterize the microstructure of the products. Chemical-state analysis was carried out by X-ray photoelectron spectroscopy (XPS, Thermo Scientific) with Al Kα radiation as the excitation source. Time-depended photoresponse of the devices was measured using a CHI660E electrochemical workstation in the light source of a range of wavelengths (365 nm, 470 nm, 530 nm, 625 nm, 850 nm, 940 nm).

3. RESULTS AND DISCUSSIONS

3.1. XRD and XPS Analysis

Figure **1** shows the XRD patterns of the BP samples. Most of the diffraction peaks at the two theta of 24.01°, 29.24°, 31.79°, 32.54°, 44.30°, 46.67°, 56.21° and 57.59° could be indexed to the orthorhombic phase of Bi_2O_2Se (PDF#73–1316) with a space group of I4/mmm, correspond to (101), (004), (103), (110), (114), (200), (116) and (213) planes of Bi_2O_2Se, respectively. Besides, the three weak peaks

at the two theta of 27.39°, 40.06°, 52.37° is assigned to (120), (220), ($\bar{3}21$) planes of monoclinic Bi_2O_3 (PDF#71-0465), indicating the existence of trace impurity in BP samples. Based on the intensity of the diffraction peak, the amount of impurity Bi_2O_3 gradually decreases with the increase of PVP content and the sample BP-3 is single-crystalline Bi_2O_2Se nanosheets, which demonstrates that PVP plays an important role in the growth of Bi_2O_2Se nanosheets. This was revealed later in the discussion.
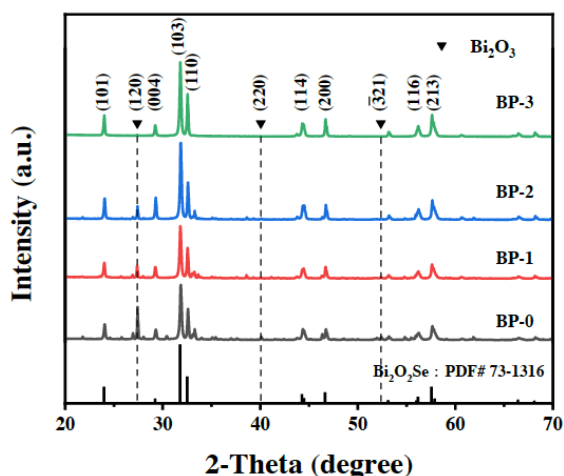

Figure 1: XRD pattern of BP samples.

The elemental composition and chemical states of the samples were further characterized by XPS. It can be seen from the full spectrum of XPS in Figure **2a** that there are four elements Bi, Se, O and C. The fine spectrum of Bi 4d, Se 3d and O 1s are shown in Figure **2b-d**. The peaks of Bi $4f_{5/2}$ and Bi $4f_{7/2}$ are centered at 163.4 eV and 158.1 eV, which can be referred to the existence of Bi^{3+}. The two peaks at 53.7 eV and 52.7 eV in the Se 3d spectrum can be attributed to the Se $3d_{3/2}$ and Se $3d_{5/2}$ states. The positions of the two peaks in the O1s spectrum are 530.8 eV and 529.1 eV. All these binding energies are consistent with the elements in Bi_2O_2Se, indicating that high-quality Bi_2O_2Se nanosheets have been synthesized.

3.2. Morphology

The morphology of BP samples is displayed in Figure **3a-d**. As-synthesized Bi_2O_2Se presents rectangular plate-like structure in agreement with its tetragonal phase, but the size of Bi_2O_2Se nanosheets varies within a wide range of 0.1~1 μm. As is showed in Figure **3e**, the average lateral dimension of the samples and the half peak width of size distribution both diminishes with the increase of PVP; the former is 238.9 nm, 192.4 nm, 179.8 nm, 176.3 nm, respectively, the latter indicates that the sample tends to be uniform
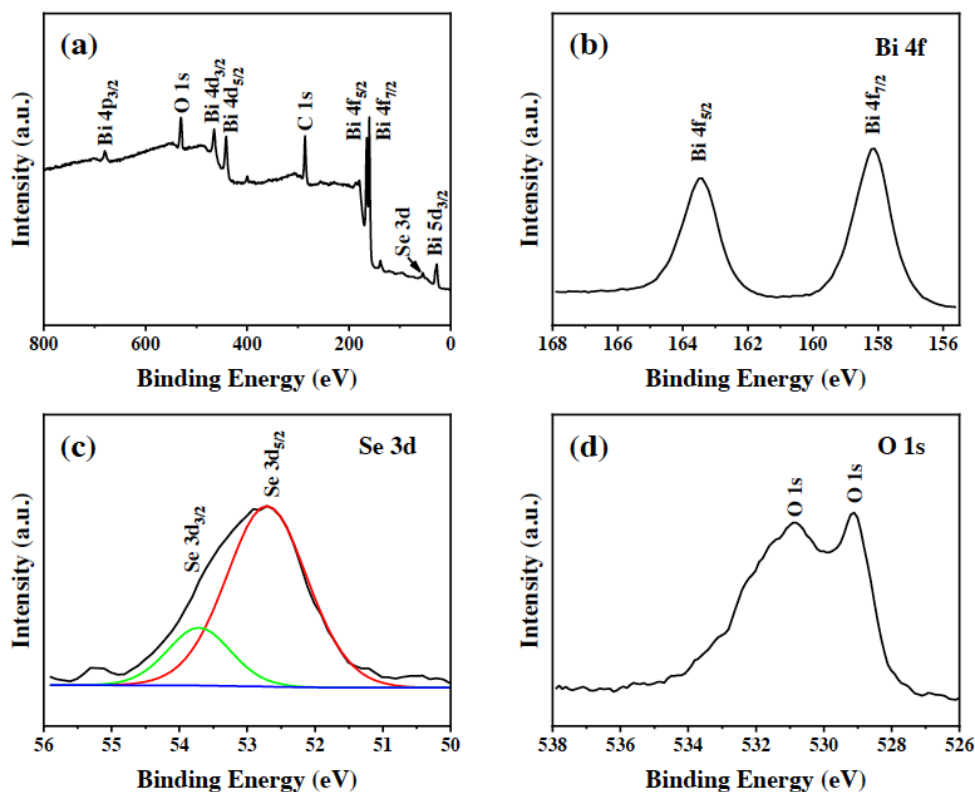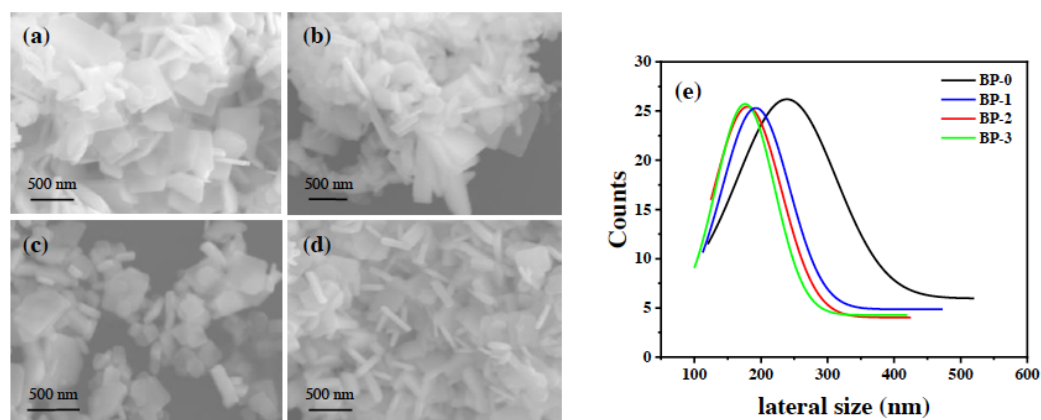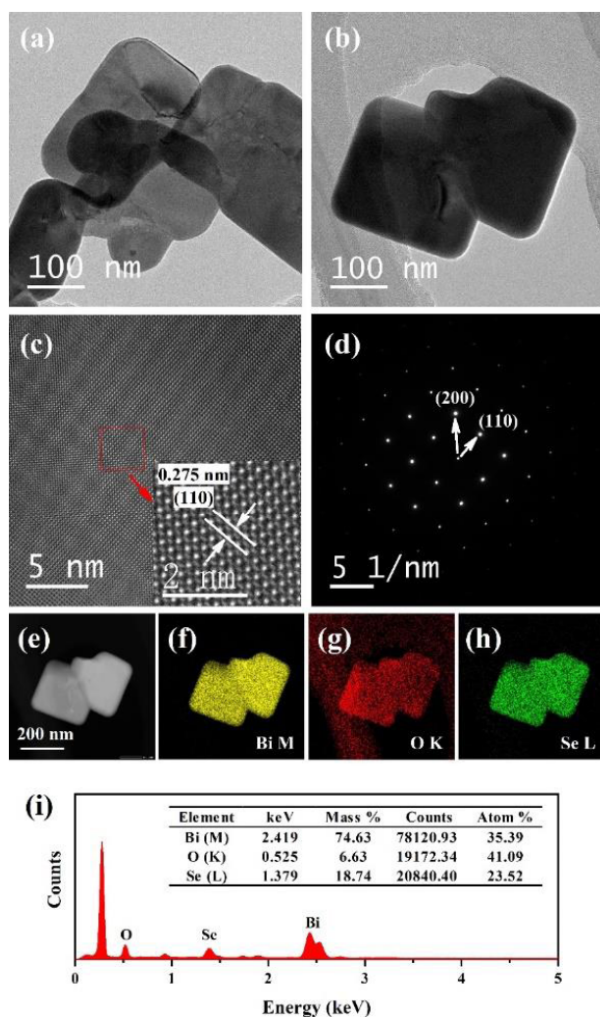

Figure 2: XPS spectra of the BP-3 sample: (**a**) XPS survey pattern of the BP-3 sample, (**b**) XPS spectra of the Bi 4f, (**c**) XPS spectra of the Se 3d, and (**d**) XPS spectra of the O 1s.

Figure 3: SEM images and size distribution of BP samples: (**a**) BP-0, (**b**) BP-1, (**c**) BP-2, (**d**) BP-3 and (**e**) Size distribution of BP samples (Fitting by a Gaussian function).

in size. To sum up, PVP has the capability of limiting the lateral growth of Bi_2O_2Se nanosheets and enabling them homogenized as a surfactant or dispersant in the reaction system.

Figure 4: TEM images of the BP-3 sample. (**a**, **b**) TEM; (**c**) HRTEM; and (**d**) SAED images of the Bi_2O_2Se nanosheets;

(**e**-**h**) corresponding elemental mappings of Bi, O and Se; (**i**) EDS pattern of the Bi_2O_2Se nanosheets.

To further study the crystal structure and microtopography, Bi_2O_2Se nanosheets can be transferred onto a Cu grid for transmission electron microscope (TEM) examination. The TEM images exhibit that Bi_2O_2Se nanosheets with flat surfaces show rectangular or square shape in Figure **4a-b**, which indicates good consistency with SEM measurement. A high-resolution TEM (HRTEM, Figure **4c**) image of Bi_2O_2Se shows *d*-spacings of 2.75 Å for (110) planes and a selected area electron diffraction (SAED) pattern shows (200), (110) spots and square symmetry (Figure **4d**), suggesting the formation of Bi_2O_2Se nanosheets perpendicular to the c axis. EDS analysis also provided more direct evidence for the chemical composition of Bi_2O_2Se. As shown in Figure **4e-h**, the mapping scanning reveals the uniform distributions of Bi, O and Se. It is found from Figure **4i** that EDS spectrum exists the peaks of Bi, O and Se with a Bi:Se:O chemical composition of 2:2:1 (inset of Figure **4i**)

3.3. The Optimization Mechanism of PVP

Scheme **1** displays the synthetic process of Bi_2O_2Se nanosheets. In short, $Bi(NO_3)_3 \cdot 5H_2O$ was hydrolyzed to form $[Bi_2O_2]^{2+}$ group and Se power was reduced to Se^{2-}, then the two interacted to obtain Bi_2O_2Se. The main roles of PVP in reaction systems are that 1) PVP could suppress the growth of some special crystal planes of Bi_2O_2Se nanosheets by combining the cationic $[Bi_2O_2]^{2+}$ with its carbonyl (C=O), and 2) PVP was served as a dispersant to form a large quantity of nucleation sites, which obtained small-size nanosheets because of the insufficiency of raw materials. In addition, the reason
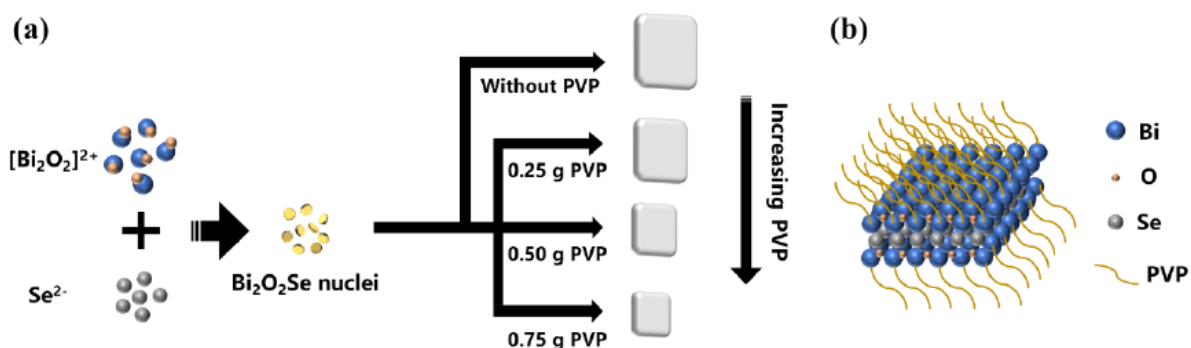
Scheme 2: Illustration of the growth of Bi$_2$O$_2$Se nanosheets.

why the impurity Bi$_2$O$_3$ existed may be that the aggregated [Bi$_2$O$_2$]$^{2+}$ group couldn't be bound with Se^{2-} and generated the precipitation of Bi$_2$O$_3$ in the conditions of no PVP or insufficient PVP.

3.4. Photoelectric Properties

To further evaluate the photoelectric properties of the samples, we fabricated the PEC-type self-powered photodetector based on Bi$_2$O$_2$Se nanosheets. Details of the device fabrication processes are described in the Experimental Section and all performance measurements of the devices were completed at a bias potential of 0 V.

Figure **5a** shows the current density of the Bi$_2$O$_2$Se devices distinguished through PVP addition amount under illumination of 365 nm ultraviolet light. It can be clearly seen that the photocurrent ($I_{ph} = I_{illuminated} - I_{dark}$) gradually decreases with the increase of PVP content in the reaction system, which can be explained that larger specific surface area lead by adding PVP content promotes the number of photons absorbed and accelerates the separation of photogenic electron hole pairs.

Response time, regarding to the rise (τ_r) and decay (τ_d) time, is one of the important indexes to evaluate device performance. The τ_r is defined as the time for the photocurrent to increase from initial value to 63% of the maximum, while the τ_d is identified as the time for the photocurrent to decline from the peak value to 37% of the maximum. In Figure **5b**, the τ_r is 9 ms and the τ_d is 12 ms, which these values are superior to those of self-powered photodetectors based on other nanomaterials (Table **1**).

To evaluate the photoelectric properties of the Bi$_2$O$_2$Se self-powered photodetector, the variation of

photocurrent of BP-3 device with power and wavelength is shown in Figure **5c-d**. Under the light power density of 15 mW/cm^2, the I_{ph} presents a downward trend from 164.4 µA/cm^2 to 37.1 µA/cm^2 as the wavelength of incident light decreases in Figure **5c**. Moreover, the device still generates a large photocurrent even in the near infrared band, such as 850 nm and 940 nm, attributed to the narrow band gap of Bi$_2$O$_2$Se that makes it absorb low-energy photons. In Figure **5c**, the I_{ph} varies along a nonlinear curve from 5 mW/cm^2 to 80 mW/cm^2, and the minimum and maximum value are 70.5 µA/cm^2 and 420.6 µA/cm^2, respectively. It is reported that the nonlinear characteristic is attributed to the complex processes including the electron–hole generation, trapping, and recombination within the semiconductor.

Responsivity (R) and detectivity (D^*), as the vital parameters to evaluate the photodetection performance of optoelectronic devices, are expressed by the following formula:

$$R = I_{ph} / PS \tag{1}$$

$$D^* = I_{ph} S^{1/2} / P S (2 e I_{dark})^{1/2} \tag{2}$$

where I_{ph} is photocurrent, I_{dark} is the dark current, P is the light intensity, S is the effective area, e is the electronic charge. As Figure **5e-f** show, R and D^* of BP-3 device maintain the same trend with the corresponding photocurrent (Figure **5c**) from ultraviolet light to near infrared light, and their values can approach up to 10.93 mA/W and 2.45 ×10^8 Jones under the illumination of 365 nm light at the light power density of 15 mW/cm^2, respectively. In the visible and near infrared regions, Bi$_2$O$_2$Se still has high responsivity and detectivity, such as 2.47 mA/W and 7.61×10^7 Jones under 940 nm, enabling the capacity of broadband photodetection. R and D^* of BP-3 device
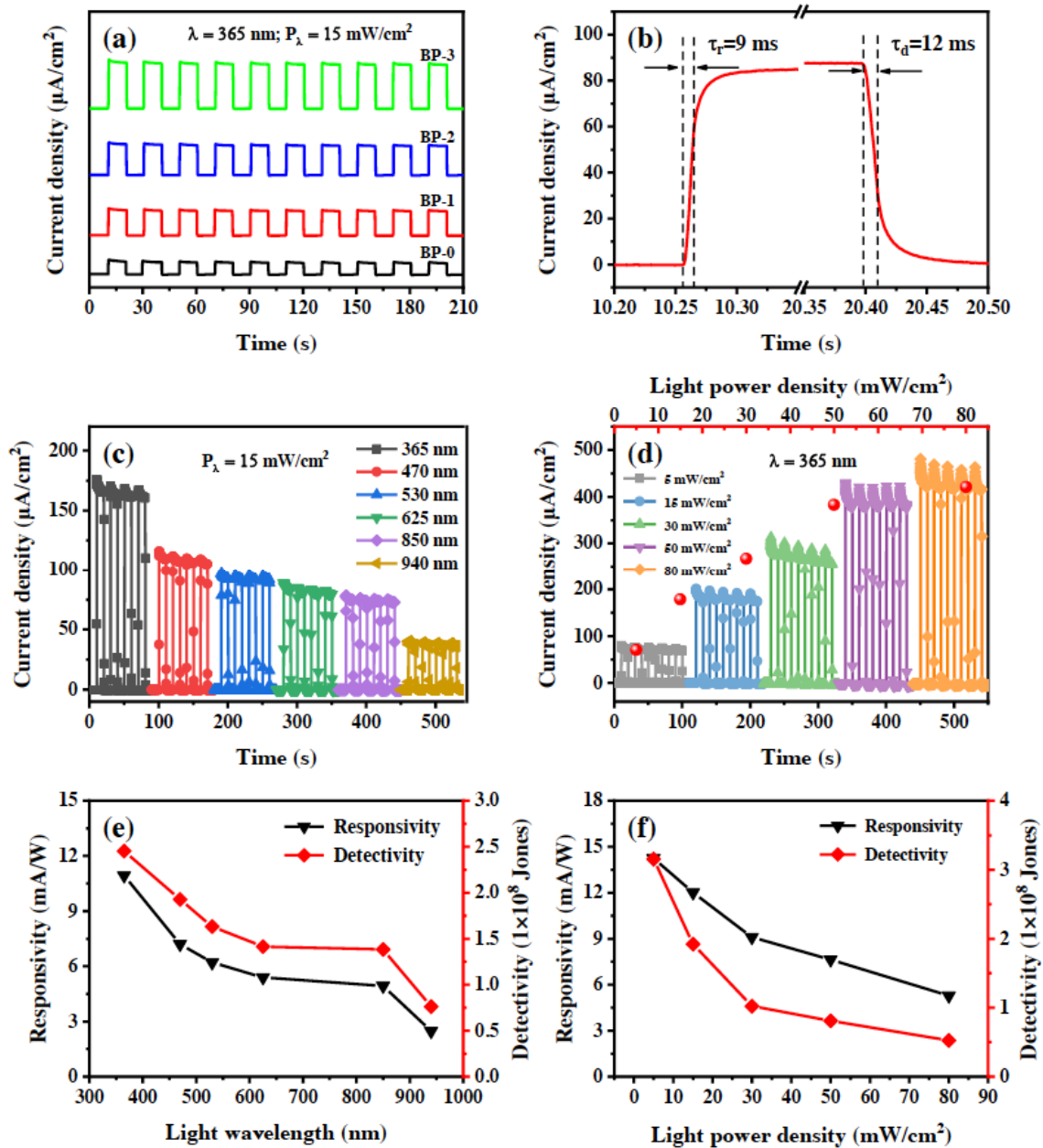
Figure 5: The photoelectric properties of the PEC-type Bi_2O_2Se self-powered photodetectors at a bias potential of 0 V. (**a**) The current density of Bi_2O_2Se devices in the light power density of 15 mW/cm^2, (**b**) The current density of BP-3 device at different light wavelengths (Light power density: 15 mW/cm^2), (**c**) The current density of BP-3 device at different light power density (light wavelength: 365 nm), (**d**) The rise and delay time of BP-3 device, (**e**)-(**f**) Responsivity and Detectivity of BP-3 device at different light wavelengths and light power density.

are the reverse with the trend of photocurrent from 5 mW/cm^2 to 80 mW/cm^2, and both reach the maximum at 5 mW/cm^2 and are 14.24 mA/W and $3.16×10^8$ Jones, respectively. This phenomenon is due to nonlinear increase of photocurrent and large dark current at high optical power density.

4 CONCLUSIONS

In summary, the Bi_2O_2Se nanosheets with small size were successfully synthesized via a facile one-

step PVP-assisted hydrothermal process for the first time. Self-powered photodetector based on Bi_2O_2Se nanosheets exhibited excellent photodetection performance with the responsivity of 14.24 mA/W and detectivity of $3.16×10^8$ Jones. This work could be hoped to play a part in the preparation of Bi_2O_2Se nanomaterials and promote the development of novel self-powered photodetectors in the future.

Table 1:   Comparison of Different Self-Powered Photodetectors Performance Based on Nanomaterials

Materials	Light source	Measurement Condition	Responsivity	Detectivity	Rise Time	Refs
Bi nanosheets	Optical-fiber source	1 M NaOH, 0.5V	≈1.8 µA W^{-1}	—	≈1.45 s	[16]
Te/Se nanotubes	Simulated light	0.5 M KOH, 0.6 V	98.8 µA W^{-1}	—	—	[17]
GaN nanowires	365 nm	Iodine electrolyte, 0 V	250 µA W^{-1}	—	0.28 s	[18]
BP nanosheets	350 W Xenon arc lamp	0.1 m KOH, 0 V	2.2 µA W^{-1}	—	0.5 s	[19]
InSe nanosheets	500 W Xenon arc lamp	0.2 m KOH, 1.0 V	4.9 µA W^{-1}	—	5.0 s	[20]
WS₂/graphene	350 W Xenon arc lamp	Solid polymer gel electrolyte, 0 V	46.7 µA W^{-1}	—	1.2 s	[21]
Bi₂O₂S nanoplates	150 W xenon lamp	0.5 M KOH, 0.6 V	2.31 mA W^{-1}		80 ms	[22]
Bi₂O₂Se nanosheets	365 nm	Sulfur electrolyte, 0V	14.24 mA W^{-1}	3.16×10^8 Jones	9.0 ms	This work

REFERENCES

[1]   Zhao B, Wang F, Chen HY, Zheng LX, Sun Lx, Zhao DX, Fang XS. An Ultrahigh Responsivity (9.7 mA W-1) Self-Powered Solar-Blind Photodetector Based on Individual ZnO-Ga2O3 Heterostructures. Advanced Functional Materials 2017; 1700264.
https://doi.org/10.1002/adfm.201700264

[2]   Ni SM, Guo FY, Wang DB, Liu G, Xu ZK, Kong LP, Wang JZ, Jiao SJ, Zhang Y, Yu QJ, Luo JW, Wang B, Li ZH, Zhang CC, Zhao LC. Effect of MgO Surface Modification on the TiO2 Nanowires Electrode for Self-Powered UV Photodetectors. ACS Sustainable Chem. Eng 2018; 7265-7272.
https://doi.org/10.1021/acssuschemeng.7b04188

[3]   Qiao H, Huang Zy, Ren Xh, Liu Sh, Zhang Yp, Qi X, Zhang H. Self-Powered Photodetectors Based on 2D Materials. Advanced optical materials 2020; 1900765.
https://doi.org/10.1002/adom.201900765

[4]   Zhou JY, Chen LL, Wang YQ, He YM, Pan XJ, Xie EQ. An overview on emerging photoelectrochemical self-powered ultraviolet photodetectors. Nanoscale 2016; 50-73.
https://doi.org/10.1039/C5NR06167A

[5]   Lee E, Yoo H. Self-Powered Sensors: New Opportunities and Challenges from Two-Dimensional Nanomaterials. Molecules, 2021; 5056.
https://doi.org/10.3390/molecules26165056

[6]   Wu XF, Sun J, Shao H, Zhai Y, Li LF, Chen WD, Zhu JY, Dong B, Xu L, Zhou DL, Xu W, Song HW, Bai X. Self-powered UV photodetectors based on CsPbCl3 nanowires enabled by the synergistic effect of acetate and lanthanide ion passivation. Chemical Engineering Journal 2021; 131310.
https://doi.org/10.1016/j.cej.2021.131310

[7]   Ren XH, Li ZJ, Huang ZY, Sang D, Qiao H, Qi X, Li JQ, Zhong JX, Zhang H. Environmentally Robust Black Phosphorus Nanosheets in Solution: Application for Self-Powered Photodetector 2017; 1606834.
https://doi.org/10.1002/adfm.201606834

[8]   Cong RD, Qiao S, Liu JH, Mi JS, Yu W, Liang BL, Fu GS, Pan CF, Wang SF. Ultrahigh, Ultrafast, and Self-Powered Visible-Near-Infrared Optical Position-Sensitive Detector Based on a CVD-Prepared Vertically Standing Few-Layer MoS2/Si Heterojunction. advanced science, 2018; 1700502.
https://doi.org/10.1002/advs.201700502

[9]   XS. Li, WW. Cai, J. An, SY. Kim, J. Nah, DX. Yang, R. Piner, V. Aruna, I. Jung, E. Tutuc, S. K. Banerjee, L. Colombo, R. S. Ruoff, Large-Area Synthesis of High-Quality and Uniform Graphene Films on Copper Foils. Science 2009; 324: 1312.
https://doi.org/10.1126/science.1171245

[10]   Yin JB, Tan ZJ, Hong H, Wu JX, Yuan HT, Liu YJ, Chen C, Tan CW, Yao FR, Li TR, Chen YL, Liu ZF, Liu KH, Peng HL. Ultrafast and highly sensitive infrared photodetectors based on two-dimensional oxyselenide crystals. Nature Communication 2019; 3457.
https://doi.org/10.1038/s41467-019-11422-3

[11]   Chen GX, Wu J, Wang B, Li J, Qi X, High-performance self-powered photodetector based on Bi2O2Se nanosheets. Applied Physics A-Materials Science & Processing 2020; 126.
https://doi.org/10.1007/s00339-020-03759-0

[12]   Luo P, Wang FK, Qu JY, Liu KL, Hu XZ, Liu KW, Zhai TY. Self-Driven WSe2/Bi2O2Se Van der Waals Heterostructure Photodetectors with High Light On/Off Ratio and Fast Response. Advanced Functional Materials 2021; 2008351.
https://doi.org/10.1002/adfm.202008351

[13]   Liang SQ, Zhou J, Liu J, Pan AQ, Tang Y, Chen T, Fang GZ. PVP-assisted synthesis of MoS2 nanosheets with improved lithium storage properties. Crystengcomm 2013; 4998-5002.
https://doi.org/10.1039/c3ce40392k

[14]   Ding SP, Xiong XY, Liu XF, Shi YQ, Jiang QQ, Hu JC. Synthesis and characterization of single-crystalline Bi2O2SiO3 nanosheets with exposed {001} facets. Catalysis Science &Technology 2017; 3791-3801.
https://doi.org/10.1039/C7CY01291H

[15]   Wang XM, Li JM, Liu WF, Yang SF; Zhu CF, Chen T. A fast chemical approach towards Sb2S3 film with a large grain size for high-performance planar heterojunction solar cells. Nanoscale 2017; 3386-3390.
https://doi.org/10.1039/C7NR00154A

[16]   Huang H, Ren XH, Li ZJ, Wang HD, Huang ZY, Qiao H, Tang PH, Zhao JL, Liang WY, Ge YQ, Liu J, Li JQ, Qi X, Zhang H. Two-dimensional bismuth nanosheets as prospective photo-detector with tunable optoelectronic performance. Nanotechnology 2018; 23.
https://doi.org/10.1088/1361-6528/aab6ee

[17]   Huang WC, Zhang Y, You Q, Huang P, Wang YZ, Huang ZYN, Ge YQ, Wu LM, Dong ZJ, Dai XY, Xiang YJ, Li JQ,

Zhang XW, Zhang H. Enhanced Photodetection Properties of Tellurium@Selenium Roll-to-Roll Nanotube Heterojunctions. Small 2019; 1900902.
https://doi.org/10.1002/smll.201900902

[18]   Zhang MX, Liu Y, Yang MQ, Zhang W, Zhou JY, Zhang ZX, Xie EQ, Pan XJ, Li SB. High performance self-powered ultraviolet photodetectors based on electrospun gallium nitride nanowires. Applied Surface Science 2018; 43-48.
https://doi.org/10.1016/j.apsusc.2018.04.225

[19]   Ren XH, Li ZJ, Huang ZY, Sang D, Qiao H, Qi X, Li JQ, Zhong JX, Zhang H. Environmentally Robust Black Phosphorus Nanosheets in Solution: Application for Self-Powered Photodetector. Advanced Functional Materials 2017; 1606834.
https://doi.org/10.1002/adfm.201606834

[20]   Li ZJ, Qiao H, Guo ZN, Ren XH, Huang ZY, Qi, X, Dhanabalan SC, Ponraj JS, Zhang D, Li JQ, Zhao, JL, Zhong

JX, Zhang H. High-Performance Photo-Electrochemical Photodetector Based on Liquid-Exfoliated Few-Layered InSe Nanosheets with Enhanced Stability. Advanced functional Materials 2018, 1705237.
https://doi.org/10.1002/adfm.201705237

[21]   Ren XH, Wang B, Huang ZY, Qiao H, Duan CG, Zhou Y, Zhong JX, Wang ZY, Qi X. Flexible self-powered photoelectrochemical-type photodetector based on 2D WS2-graphene heterojunction. Flat Chem 2021; 100215.
https://doi.org/10.1016/j.flatc.2020.100215

[22]   Wang K, Qiao H, Li J, Qi X. A robust photoelectrochemical photodetectors based on the self-healing properties of Bi2O2S nanoplates. Applied Surface Science 2021; 150444.
https://doi.org/10.1016/j.apsusc.2021.150444